Ultramicroscopy 47 (1992) 425–436
North-Holland

ultramicroscopy

Evolution of microstructure and magnetic properties in magnetron-sputtered CoCr thin films

B.G. Demczyk

North Campus EMAL, Department of Materials Science and Engineering, The University of Michigan, Ann Arbor, MI 48109-2143, USA

Received at Editorial Office 13 July 1992

The microstructure and magnetic-structure development in magnetron-sputtered Co–22at%Cr thin films deposited on amorphous substrates has been examined systematically and in detail. It has been found that the initial deposit is amorphous up to a thickness of ~ 5 nm. By 10 nm thickness, a polycrystalline highly hcp c-axis textured (out of the film plane) microstructure is observed. At 50 nm thickness, a distinct columnar morphology has developed. A distinct subgrain structure was also observed in the thinner films (10–50 nm). The magnetization is initially in-plane and retains in-plane components up to a thickness of ~ 50 nm, after which it is predominantly out-of-plane. The effects of in-plane film stress are reflected in the effective anisotropy field and are most evident in the thinner films, where the stress is highest. The thinnest (10 nm) films display in-plane 180° domain walls while thicker (50 nm) films exhibit out-of-plane "dot"-type domain structures. The "dot" domains were observed even in films that had not yet developed a columnar morphology. Intermediate-thickness films show a "feather-like" contrast, indicating that both in- and out-of-plane magnetization components are present. Intrinsic film stress was found to play a major role in determining the preferred magnetization direction and, thus, the resulting magnetic domain configurations.

1. Introduction

CoCr thin films have been considered for a number of years as the leading candidate for perpendicular recording media [1,2]. There have been a number of reviews [3–9] of the film microstructure and magnetic properties. Generally, these studies have concluded that the development of a columnar microstructure with a strong hcp c-axis texture perpendicular to the film plane occurs concurrently with the observation of a large positive magnetocrystalline anisotropy favoring magnetization normal to the film plane. In this investigation, the development of the microstructure in Co–22at%Cr films sputter-deposited on amorphous substrates has been examined in considerably more detail than has been reported to date. We have also measured the saturation magnetization and anisotropy field as well as the as-deposited in-plane film stress for films in the thickness range 10–500 nm to determine their contribution to the overall film anisotropy. Finally, the evolution of the magnetic domain structures in films of known microstructure were examined by Lorentz transmission electron microscopy. Observations were related to the measured stress values to illustrate the effects of the latter on the net magnetization and, thus, the resulting magnetic domain structures in these films.

2. Experimental details

Films were sputtered from a 12.5 cm diameter Co–22at%Cr alloy target using a Varian DC magnetron ("S" gun) sputtering system. Sputtering conditions included an argon pressure of one mTorr, unheated substrates ($T < 50°C$) and a sputtering rate of 0.25 nm/s. Thin-film (≤ 50 nm) plan-view TEM specimens were prepared by depositing directly onto carbon-coated 3 mm cop-

0304-3991/92/$05.00 © 1992 – Elsevier Science Publishers B.V. All rights reserved

per grids, permitting direct TEM observation. Thicker films were deposited onto glass (Corning 7059) substrates which were mechanically thinned to about 40 μm, after which they were ion(Al^+)-beam-milled to electron transparency. The similarity of microstructures for thick (> 50 nm) films deposited on amorphous carbon and glass substrates has been reported previously [8]. Section samples (deposited on glass) were fabricated by bonding two films face-to-face, mechanical thinning, and ion-beam milling. Conventional TEM (bright-field imaging and selected-area diffraction) as well as electron microdiffraction were performed on a JEOL 2000FX transmission electron microscope operating at 200 kV. For high-resolution work, a JEOL 4000EX HREM operating at 400 kV was employed. X-ray rocking ($\Delta\theta_{50}$) curves were taken utilizing Cu Kα radiation on a Rigaku Geigerflex diffractometer. In-plane stress measurements were made using a cantilever beam-deflection method [10] in which the substrate (glass) curvature due to film stress is measured. For this work, samples were cut into 6.35 mm × 25.4 mm strips and scanned with a laser beam over their entire length, after which the metal film was removed via etching in aqua regia and the glass substrate alone scanned again. In this way, the effects of inherent substrate curvature could be removed from the measurement. Vibrating-sample magnetometry (VSM) was performed on 49 mm^2 samples with a Princeton Applied Research Model 155 magnetometer, using a saturation field of 15 kOe. Ferromagnetic resonance (FMR) curves were taken on 1 mm^2 samples using a 33 GHz resonant cavity system [11] for which the maximum field was 19 kOe. Magnetic domains were imaged in the Fresnel Lorentz TEM mode [12]. In this mode of opera-

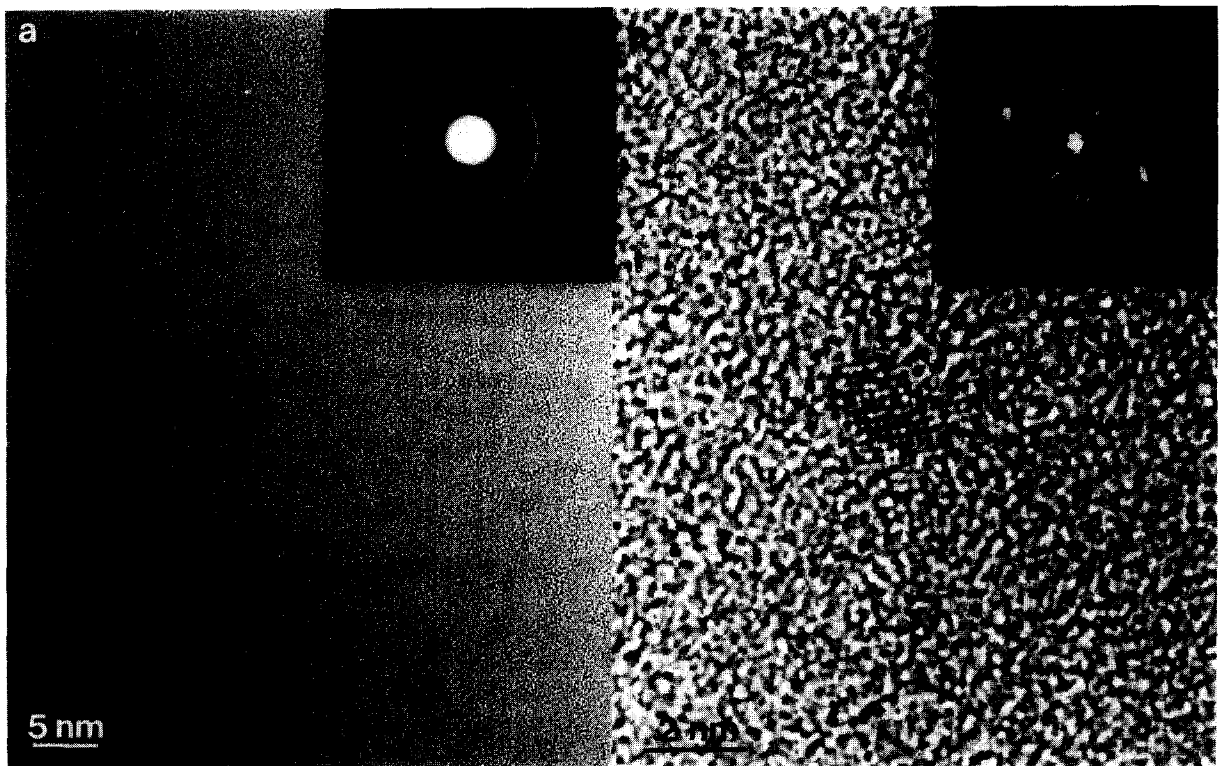

Fig. 1. (a) TEM micrograph of a 5 nm thick CoCr film. Note the presence of occasional small crystallites within the amorphous matrix. Arrow indicates one such crystallite. (b) HREM image showing a single crystallite. Inset depicts the corresponding optical diffraction pattern.

tion, the field applied by the microscope objective lens at the back focal plane was less than 5 Oe.

3. Results

3.1. Microstructural details

Fig. 1 shows a plan-view high-resolution micrograph taken from a 5 nm thick CoCr film. As shown, the greater part of the area is "amorphous", even at the approximately 0.18 nm point-to-point resolution of the microscope. The ring pattern taken from this area (fig. 1a inset), although sharp, displays no discrete diffraction maxima and is consistent with an amorphous structure. Small (~ 2 nm) crystallites are occasionally observed within the amorphous matrix (arrowed in fig. 1a). Fig. 1b shows a high-resolution image of a single crystallite. The optical diffraction pattern (Fourier transform of image) taken from a similar region (fig. 1b inset) shows evidence of crystallinity as indicated by the presence of discrete diffraction spots. These results represent the first actual observation of the initial crystallite nucleation layer in CoCr thin films.

Figs. 2a–2d show typical plan views of the microstructure for films of thickness 10–500 nm. From fig. 2a, it can be seen that by 10 nm, grain structure is starting to develop. In thicker films,

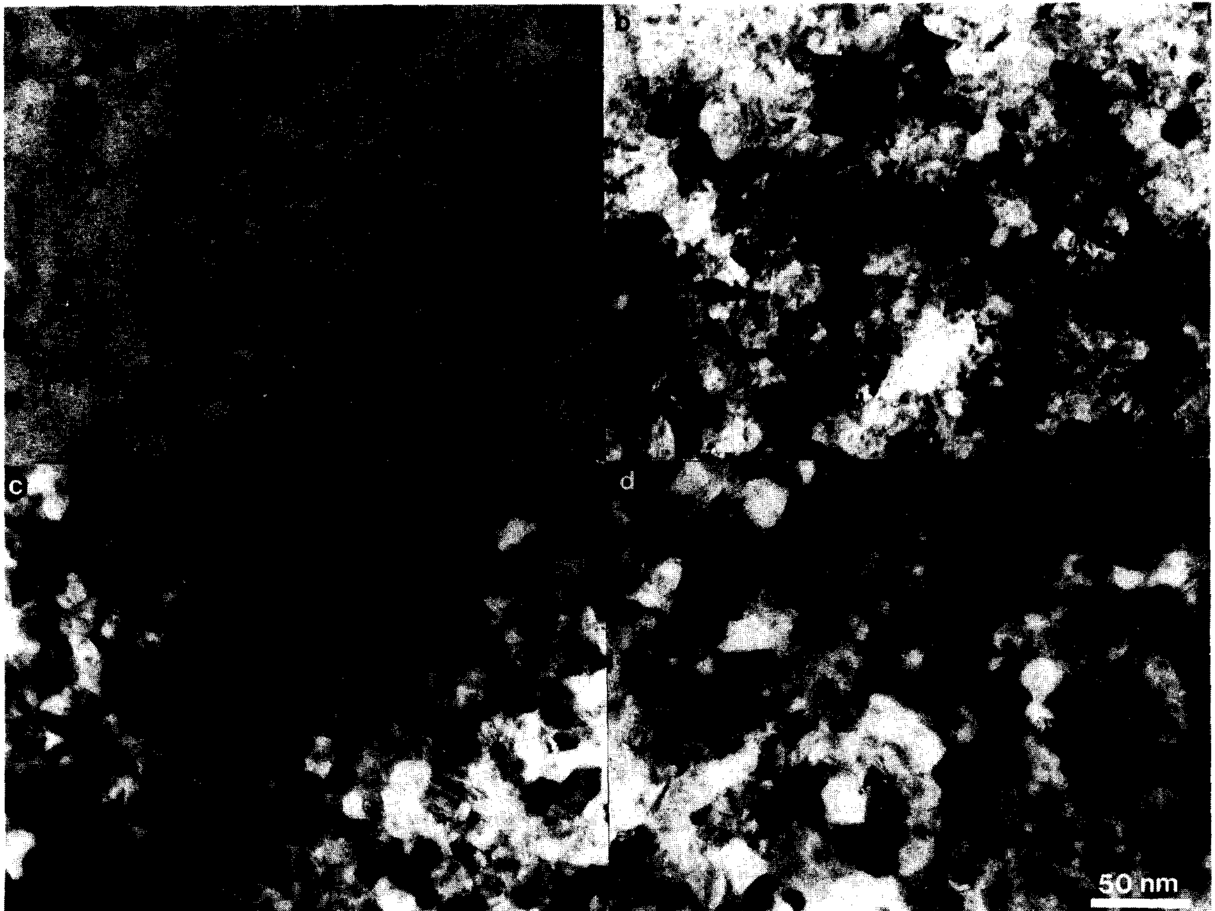

Fig. 2. TEM micrographs (plan view) of (a) 10 nm, (b) 50 nm, (c) 100 nm, (d) 500 nm thick CoCr films. Note the presence of intragranular defects in (c) and (d).

these grains become more pronounced (figs. 2b–2d). In addition, defects are observed within individual grains. These have been shown to be stacking faults, lying on the (0001) planes [13]. Since similar faults have been found in CoNiCr films that do not display c-axis texture normal to the film plane, as well [13], they are not formed as a result of a mis-stacking of c planes. Therefore, it is thought that these faults form to relieve the large in-plane film stress developed in film growth. From table 1, we see that the average grain diameter is nearly constant with increasing film thickness, indicating that the final grain size is reached early on (by 50–100 nm thickness). This result differs from that reported in refs. [9,14–17], in which the grain size increased with increasing film thickness over a considerable film-thickness range, but is similar to the results presented in refs. [18,19]. Figs. 3a–3d show the corresponding selected-area diffraction patterns taken from these films. Note that in all of the patterns, only rings of the form {$hki0$} are present, which indi-

Table 1
Film [a] orientation parameters

t (nm)	d_g (nm)	d_c (nm)	$\Delta\theta_{50}$ (deg)	α_{avg} (deg)
10	19	–	–	10.1
50	19	24	9.6	12.3
100	20	16 –55	9.5	13.5
500	21	19.5–31	6.7	13.4

[a] All films deposited on glass substrates.
Key: t = film thickness,
d_g = average grain diameter,
d_c = column diameter,
$\Delta\theta_{50}$ = X-ray rocking curve half width,
α_{avg} = average grain-to-grain misorientation.

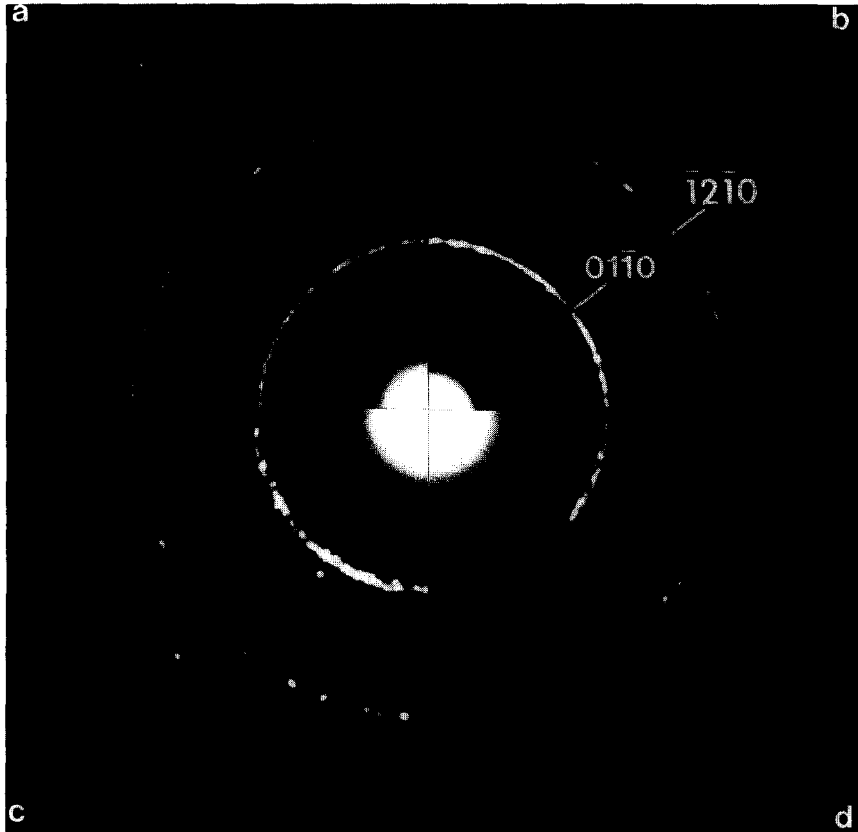

Fig. 3. SAD ring patterns taken from (a) 10 nm, (b) 50 nm, (c) 100 nm, (d) 500 nm thick CoCr films. Note that all patterns are similar.

Fig. 4. TEM micrographs (section views) of (a) 10 nm, (b) 50 nm, (c) 100 nm, (d) 500 nm thick CoCr films. Note the lack of column development in (a) and the presence of intragranular defects in (b–d).

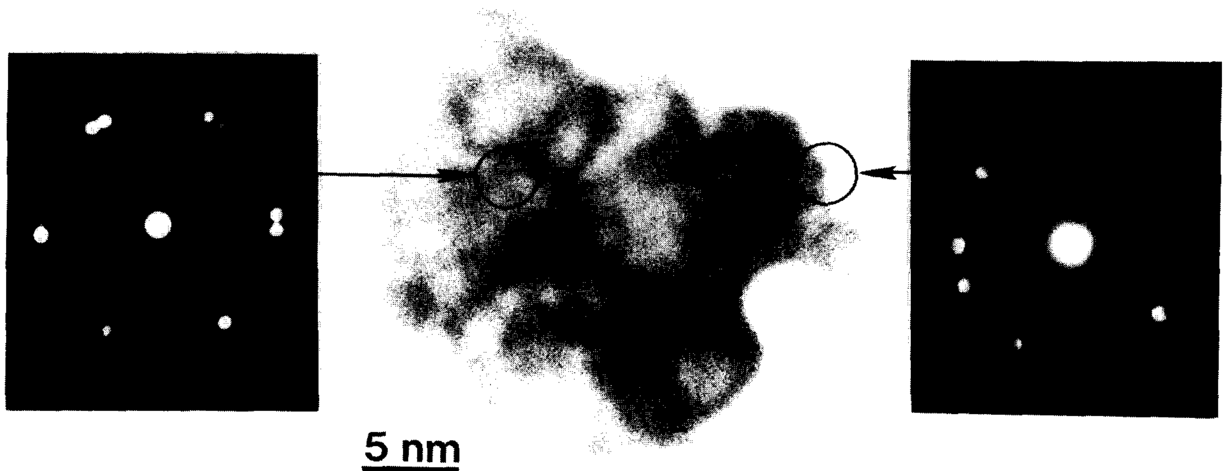

Fig. 5. Micrograph showing a single grain in a 10 nm thick CoCr film. Note the distinct boundaries within the grain. Insets represent electron microdiffraction patterns (10 nm probe size), taken across both low angle and grain boundaries.

cates c-axis (0002) texturing normal to the film plane. This is also reflected in the observed X-ray rocking (about the (0002) peak) curve half widths ($\Delta\theta_{50}$), also listed in table 1, which are 10° or less for all films for which an appreciable signal could be obtained.

In fig. 4, cross-section views are shown for these same films. At 10 nm film thickness (fig. 4a), a continuous film is observed, with no distinguishable grain structure evident. This is consistent with the plan-view microstructure for films of this thickness, in which the grains are barely distinguishable (fig. 2a). It is significant to note that these films are very strongly textured (c-axis normal to the film plane), even though a columnar microstructure has not yet developed. By 50 nm (fig. 4b), a well defined column structure has formed. These columns are seen to extend through the film thickness, even in the thicker films (figs. 4c and 4d). From table 1, we see that the range of measured column diameters is similar to the average grain diameter encountered earlier. Thus it appears that each column is comprised of a single grain, as can be inferred from the work of Hong et al. [18] for magnetron-sputtered CoCr films on fused quartz. Note also that the surface roughness increases as the film thickness increases (figs. 4c and 4d). This has been confirmed by recent atomic force microscopy results as well. The aforementioned intragranular defects are also clearly visible in films of thickness 50 nm and greater (figs. 4b–4d). At a film thickness of 500 nm (fig. 4d), the stacking fault density becomes quite high.

Close examination of the film microstructure in 10 nm films (fig. 5) reveals the presence of boundaries within the grains themselves. Electron microdiffraction (10 nm probe size) patterns taken across such boundaries (fig. 5 upper inset) reveal a small ($< 10°$) rotational misorientation, looking down the (0002) zone axis. This is to be contrasted with microdiffraction patterns taken across the grain boundaries themselves (fig. 5 lower inset), which display larger misorientations. It should be noted that the rotational misorientation may include both a-axis and components of c-axis misorientation in the film plane. The presence of these boundaries is also independently suggested from electrical resisivity measurements that display anomalously high values in the thinnest films [20]. The frequency of occurrence of these small-angle boundaries decreases with increasing film thickness.

3.2. Film stress

To qualitatively assess the contribution of the film stress to the anisotropy field, the in-plane film stress was measured. The following equation relating the stress to the measured curvature values was utilized [21].

$$\sigma = \frac{E_s t_s^2 \kappa_f}{6(1-\nu_s) t_f}, \tag{1}$$

where E_s and ν_s are Young's modulus and the Poisson ratio of the substrate, t_s and t_f are the substrate and film thickness, respectively, and κ is the curvature of the film.

It was found that the (tensile) stress in the 50 nm thick films was larger in magnitude than that in thicker films and, furthermore, that the stress was compressive in the 10 nm films. Results of in-plane film stress measurements are shown in fig. 6. It should be noted that the error in measurement for films ≥ 50 nm in thickness is estimated at no more than 10%. From this figure it is seen that there exists a large in-plane tensile

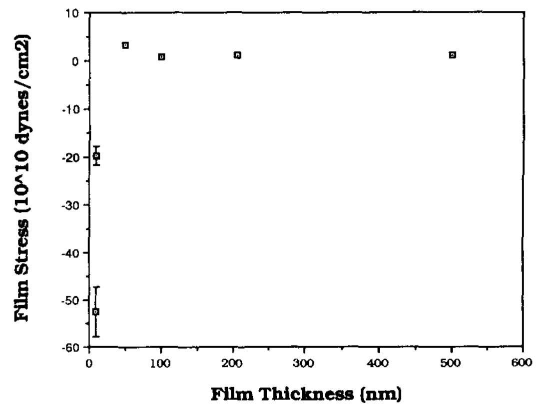

Fig. 6. In-plane film stress as a function of film thickness. Note that the 10 nm thick film stress computation was made using an average substrate curvature. The error bars indicate the error introduced by this method. See text for details.

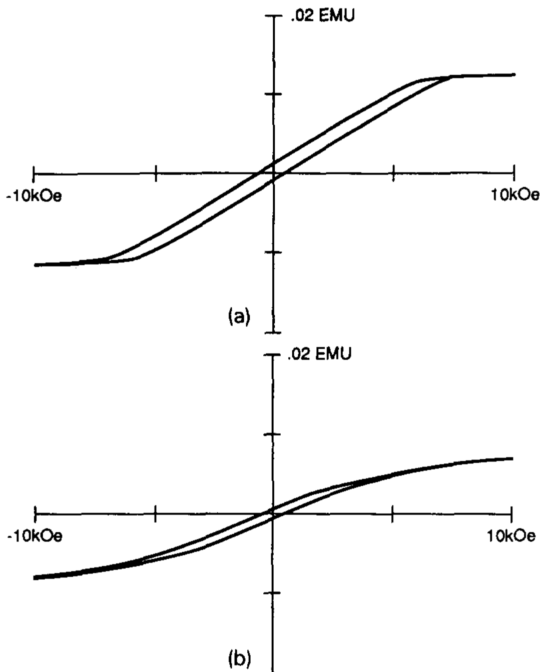

Fig. 7. Typical (a) out-of-plane and (b) in-plane VSM traces for a 500 nm thick CoCr film.

stress in all films ≥ 50 nm in thickness. This is in agreement with the results of Mitchell et al. [22] that showed a high tensile stress in 500 nm thick DC magnetron-sputtered CoCr films of the same composition. In the present case, we have observed an increase in tensile film stress at the 50 nm film thickness level. In the case of the 10 nm thick films alone, the film could not be dissolved away completely in aqua regia. Therefore, the film stress was bracketed by using both the maximum and minimum substrate curvature values measured for the other samples. We see that both stress values, computed for the 10 nm thick film, are clearly larger in magnitude and opposite in sign compared to the values for the other film thicknesses.

3.3. *M–H loops*

Figs. 7a and 7b show typical out-of-plane and in-plane hysteresis loops as measured by the VSM for a 500 nm thick film deposited on glass. The curve shapes indicate that the easy direction is out-of-plane and the hard direction, in-plane. A sheared easy axis loop (fig. 7a) could arise if the film was considered to be a multi-particle medium, in which individual columns or groups of columns comprise single domains [2]. Magnetization reversal in this case would involve the switching of a single column or clusters of columns. A sheared loop could also arise if the film reversed by domain wall motion. However, Wuori [23] has reported that calculations of the film coercivity based upon a domain-wall motion-reversal mechanism are not in agreement with measured out-of-plane coercivity values in CoCr films. This would suggest that the single (or groups of) column(s) switching mechanism is operative for fields applied perpendicular to the film plane (parallel to the easy axis). It is reasonable that the column boundaries would act to isolate magnetic domains, both from the standpoint of Cr segregation at the column boundaries, as has been reported by Chapman et al. [24], and from structural considerations. We believe that the columns are separated by high-angle ($> 10°$) boundaries (i.e. boundaries separating regions wherein the *a*-axes are misoriented by an angle greater than 10°) and it is there that domain walls can reside, as described below. The hard axis loop (fig. 7b) is seen to consist of a large linear region that distinctly kinks over at higher fields. This seems to indicate a mixed mode of magnetization reversal in which both wall motion and rotation are involved. These curve shapes were typical of all films ≥ 50 nm in thickness. In the thinnest (10 nm) films, the out-of-plane loop (fig. 8a) is the hard axis loop, while the in-plane loop (fig. 8b) is the easy axis one, indicating an in-plane magnetization, most likely arising from domain wall motion. The *M–H* loops are also consistent with FMR results [25]. Table 2 shows in-plane and out-of-plane values of the magnetic moment, M_s, measured as a function of film thickness. The error bars were established via consideration of the error involved in manually extrapolating M_s values from the experimental M versus H curves. In addition, inaccuracies in the determination of the film thickness would also affect the calculated M_s. M_s values are seen to be approximately constant (296 ± 18 emu/cm^3) with film thickness, as

has been reported in RF-sputtered CoCr films [24].

3.4. Domain configurations

Figs. 9a–9d illustrate the magnetic domain structures of the as-deposited, demagnetized specimens. At 10 nm thickness (fig. 9b), one observes well defined 180°-type domain walls bounding in-plane domains which are quite large (≥ 500 nm) with respect to the microstructural features of the film, as noted above. These results are similar to those reported by Lee et al. [27] in "amorphous" CoCr films. In the present case, however, the film is polycrystalline and highly textured with the c-axes normal to the film plane. Thus, it is the shape anisotropy field ($4\pi M_s$) that gives rise to the predominantly in-plane anisotropy, since the magnetocrystalline anisotropy ($2K_u/M_s$), directed along the hcp c-axis, would favor magnetization out of the film plane. Here, K_u represents the uniaxial anisotropy constant. In the 50 nm thick films, a "dot-like" domain structure is observed (fig. 9d). Ohkashi et al. [28] propose that this type of contrast can arise from a region of primarily out-of-plane magnetization surrounded by regions with in-plane components (for flux closure across the boundary). These in-plane components are thought to give rise to the observed wall contrast. The size of the dot-like regions varies from region to region for a given defocus value of the objective lens of the microscope, indicating that the in-plane magnetization components vary in magnitude locally [12]. Films of intermediate thickness (~ 10–20 nm) show a "feather-like" domain structure (fig. 9c, and, faintly, fig. 9b). According to Chen [29], this structure results from local variations of the in-plane magnetization. Close inspection of fig. 1c reveals that a "dot" contrast is present as well. Thus positive anisotropy magnetic constituents are also present in films of this thickness (20 nm) deposited on carbon, even though such a component could not be resolved in FMR traces of 10 nm films deposited on glass [25,30]. The electron beam, passing through the sample, sees a "volume-averaged" anisotropy distribution. Furthermore, the electron beam is deflected differently in the positive and the negative anisotropy regions, resulting in domain structure contrast representing a composite of the in-plane configuration of fig. 9b and the "dot" structure of fig. 9d. In the case of the 50 nm thick film, the greater part of the film volume consists of positive anisotropy material, and the observed domain structure is largely of the "dot" configuration. As discussed above, films of this thickness are comprised of very highly textured (c-axis normal to the film plane) grains, even though structural columns have not yet developed. This is an important point, since so much of the previous work had paid particular attention to the connection of "dot" domain structures with structural columns. The thinnest films (≤ 5 nm), which are practically amorphous, appear to have a perpendicular anisotropy component as well (fig. 9a), as has been predicted theoretically [32]. In particular, we observed a "cellular" structure of the order of several micrometers in dimension, the cell walls appearing as a well defined magnetization ripple structure. Interior re-

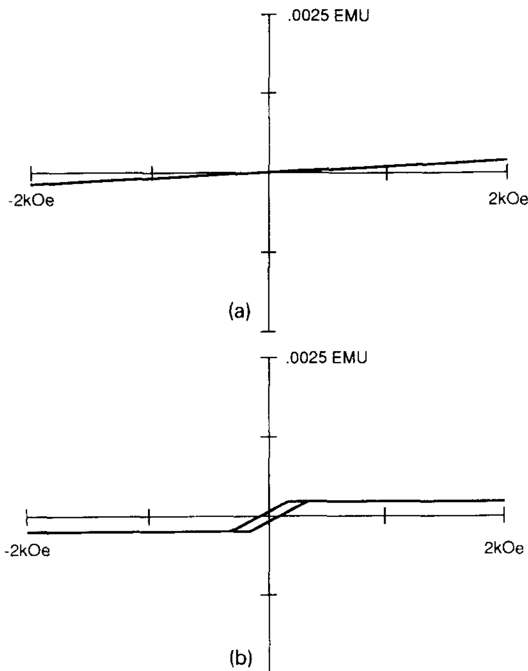

Fig. 8. Typical (a) out-of-plane and (b) in-plane VSM traces for a 10 nm thick CoCr film.

gions are seen to be comprised of a mixture of perpendicular "dot" and in-plane ripple domain contrast. This represents the first reporting of perpendicular magnetic domain contrast in very thin CoCr layers. Earlier work had reported in-plane walls with occasional magnetization ripples in amorphous films [27].

We have also computed an arbitrary "domain

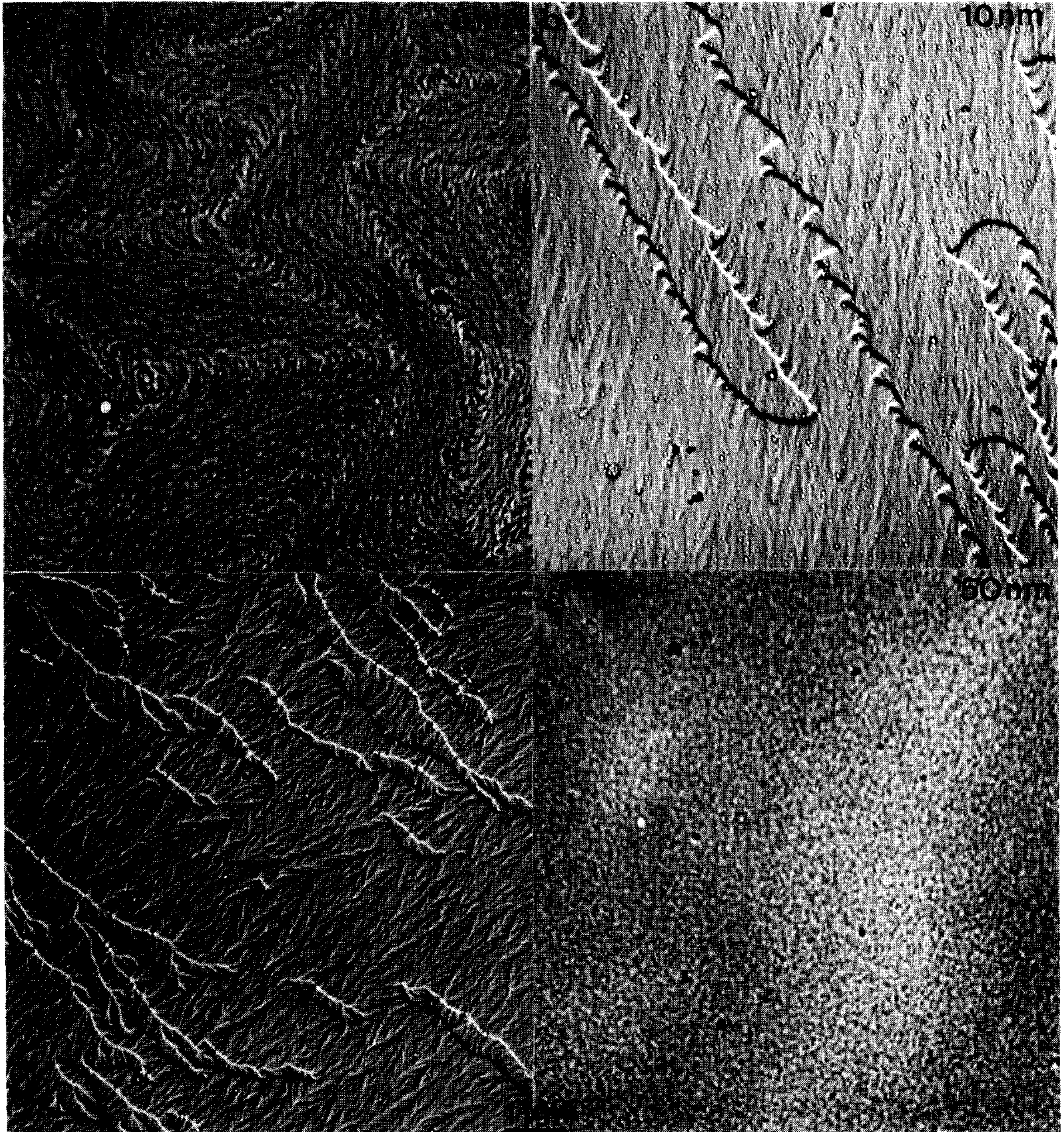

Fig. 9. Lorentz transmission electron micrographs of (a) 5, (b) 10, (c) 20 and (d) 50 nm thick CoCr thin films.

Table 2
Saturation magnetization values

t (nm)	M_s (emu/cm^2)	
	In-plane	Out-of-plane
10	283	283
50	270	272
100	310	301
205	326	321.5
500	303	295
Average	296.5 ± 18.5	

Table 3
Magnetic domain parameters (t = film thickness, l = domain wall thickness, d = domain width)

t (nm)	l (nm)	d (nm)
5	10+	100+
10	2.6	27.5
50	5.6	50

size" for samples displaying out-of-plane magnetization by subtracting twice the measured domain *wall* width from that of the *total* region encompassing the "dot" domain plus its surrounding domain walls. These values are shown in table 3 and are seen to be of the order of a few times the average grain size. Thus it appears that the film is composed of domains, comprising, at most, a few columns. This is consistent with observed easy axis hysteresis loops, which support an incoherent rotation mechanism. In-plane domain-wall widths (figs. 9b and 9c) are 10 nm or more. The spacing between domain walls for the in-plane magnetization films was found to be much larger (≥ 100 nm) than for the out-of-plane domains and is many times the observed grain size.

4. Discussion

The total measured anisotropy field can be expressed in the form:

$$H_{k\mathrm{eff}} = \frac{2K_u}{M_s} - \frac{2\sigma\lambda_s}{M_s} - 4\pi M_s, \quad (2)$$

where the terms represent the magnetocrystalline, the stress (i.e. inverse magnetostriction effect) and the shape anisotropy fields, respectively. The $H_{k\mathrm{eff}}$ value is different for each magnetically distinct region within the film. Since K_u is positive for this material [26], the magnetocrystalline anisotropy field term favors out-of-plane magnetization. From the stress anisotropy field term, we see that if λ_s is taken as negative, a positive value of σ (tensile stress) will add to the positive anisotropy field, while a negative value of σ (compressive stress) will add to the negative anisotropy field. The demagnetizing (shape anisotropy) field alone favors in-plane magnetization.

Insight into the origin of the domain structures can be gained through reexamination of eq. (2). As shown, it is the *combination* of the magnetocrystalline ($3K_u/M_s$), the shape ($4\pi M_s$) and the magnetoelastic ($3\sigma\lambda_s/M_s$) anisotropy terms that determine the preferred magnetization direction. Therefore, a significant magnetoelastic anisotropy term can swing the balance one way or the other. From above, the stresses in 50 nm thick films are seen to be tensile ($\sigma > 0$), while those in 10 nm thick films are compressive ($\sigma < 0$). For $\lambda_s < 0$ [26], a tensile stress will favor out-of-plane magnetization and a compressive stress, in-plane. In the case of the 50 nm thick film, the magnetization in the as-deposited state is found to be out of the film plane, due to both the magnetocrystalline and magnetoelastic anisotropy terms in eq. (2), and we observe the characteristic "dot" domain contrast. Therefore it is primarily the stress anisotropy that gives rise to the perpendicular anisotropy in these films. In the case of the 10 nm thick film, the intrinsic stress is compressive and the magnetoelastic anisotropy favors in-plane magnetization. Thus we observe an in-plane domain structure. At intermediate thickness values, both in and out-of-plane magnetization components are present and we observe magnetization ripple. The mechanism responsible for the "dot" contrast in the 5 nm thick films is not clear at this time and remains a topic for future investigation.

5. Summary

Experimental results on magnetron-sputtered CoCr thin films deposited on amorphous sub-

strates reveal that the initial film deposit is predominantly amorphous, with occasional small crystallites forming by the time the film has reached 5 nm thickness. These films appear to have a perpendicular anisotropy component in addition to the primarily in-plane one. At 10 nm, the film is entirely polycrystalline and already highly c-axis textured normal to the film plane. The magnetization lies primarily in-plane, and well defined in-plane 180° domain walls are observed. By 50 nm, well developed columns are seen in which one observes intragranular defects. An out-of-plane magnetization component arises in films 50 nm thick and by ~ 100 nm, most of the entire film consists of positive anisotropy (favoring M out of the film plane) material. Further growth occurs essentially in the vertical (normal to the film plane) direction. The 50 nm thick films display a "dot"-type domain configuration characteristic of a perpendicular magnetization. The domain size was found to be of the order of a few structural columns in diameter. Films of intermediate thickness show a "feather-like" structure, indicating that both in-plane and out-of-plane magnetization components are present. The anisotropy field due to the as-deposited film stress is largest for the 10 and 50 nm films and reaches a constant value in thicker films. This intrinsic film stress was seen to play a major role in promoting perpendicular anisotropy in these films and, consequently, in determining the resulting magnetic domain structures.

Acknowledgements

The author would like to thank Dr. A. Layadi and Professor J.O. Artman for helpful discussions relating to the measured magnetic properties. VSM measurements were made at the Carnegie Mellon University Data Storage Systems Center. Samples were produced by the author at Carnegie Mellon through a grant from the Division of Materials Research, National Science Foundation, Grant No. DMR-8613386.

References

[1] S. Iwasaki and Y. Nakamura, IEEE Trans. Magn. MAG-13 (1977) 1272.
[2] T. Wielinga, Investigations on Perpendicular Magnetic Recording, PhD Dissertation, Twente University of Technology, 1983.
[3] M.R. Khan and J.I. Lee, J. Appl. Phys. 63 (1988) 833.
[4] P.J. Grundy and M. Ali, J. Magn. Magn. Mater. 40 (1983) 154.
[5] Y. Uchiyama, K. Ishibashi, H. Sato, V. Hwang and T. Suzuki, IEEE Trans. Magn. MAG-23 (1987) 2058.
[6] P.A. Glocker, W.E. Yetter and J.S. Gau, IEEE Trans. Magn. MAG-12 (1986) 331.
[7] H. Hoffman, L. Kochanowski, H. Mandtl, K. Kastner, M. Mayer, W.D. Munz and K. Roll, IEEE Trans. Magn. MAG-21 (1985) 1432.
[8] J.W. Lee, B.G. Demczyk, K.R. Mountfield and D.E. Laughlin, IEEE Trans. Magn. MAG-23 (1987) 2455.
[9] C. Hwang, D.E. Laughlin, P.V. Mitchell, A. Layadi, K.R. Mountfield, J.E. Snyder and J.O. Artman, J. Magn. Magn. Mater. 54–57 (1986) 1676.
[10] D.W. Young, H. Ho, C.L. Bauer, S. Mahajan and A.G. Milnes, Mater. Res. Soc. Symp. Proc., Vol. 122 (Materials Research Society, Pittsburgh, PA, 1988) p. 573.
[11] P.V. Mitchell, A. Layadi, N.S. VanderVen and J.O. Artman, J. Appl. Phys. 57 (1985) 3976.
[12] L. Reimer, Transmission Electron Microscopy of Materials, Physics of Image Formation and Microanalysis (Springer, New York, 1984) p. 249.
[13] K. Hono, B.G. Demczyk, B.G. and D.E. Laughlin, Appl. Phys. Lett. 55 (1989) 229.
[14] J.C. Lodder, T. Weilinga and J. Worst, Thin Solid Films 101 (1983) 61.
[15] M. Futamoto, Y. Honda, H. Kakibayashi, T. Shimotsu and K. Yoshida, Jpn. J. Appl. Phys. 24 (1985) L460.
[16] P.J. Grundy, M. Ali and C.A. Faunce, IEEE Trans. Magn. MAG-20 (1984) 794.
[17] J.W. Lee, B.G. Demczyk, K.R. Mountfield and D.E. Laughlin, J. Appl. Phys. 61 (1987) 3813.
[18] M. Hong, S. Nakahara, R.B. van Dover and T. Boone, Appl. Phys. Lett. 49 (1988) 1308.
[19] H. Cura and A. Lenhart, J. Magn. Magn. Mater. 83 (1990) 72.
[20] B.G. Demczyk, J. Magn. Magn. Mater. 102 (1992) 238.
[21] R.W. Hoffman, in: Physics of Thin Films, Ed. G. Hass (Academic Press, New York, 1966), 211.
[22] P.V. Mitchell, K.R. Mountfield and J.O. Artman, J. Appl. Phys. 63 (1988) 2917.
[23] E.W. Wuori, Magnetization Reversal Mechanisms in Sputtered CoCr Films with Perpendicular Magnetic Anisotropy, PhD Dissertation, University of Minnesota, 1984.
[24] J.W. Chapman, I.R. McFadyen and J.A.C. Bernards, J. Magn. Magn. Mater. 62 (1986) 359.
[25] B.G. Demczyk and J.O. Artman, J. Phys. D (Appl. Phys.) 24 (1991) 1627.

[26] J. Worst, J.C. Lodder and T. Wielinga, Thin Solid Films 101 (1983) 75.
[27] J.W. Lee, B.G. Demczyk, K.R. Mountfield and D.E. Laughlin, J. Appl. Phys. 63 (1988) 2905.
[28] M. Ohkashi, H. Toba, S. Honda and T. Kusuda, J. Magn. Magn. Mater. 35 (1983) 266.
[29] T. Chen, IEEE Trans. Magn. MAG-17 (1981) 1181.
[30] P.V. Mitchell, A Ferromagnetic Resonance Study of Co-Cr Thin Films, PhD Dissertation, Department of Physics, Carnegie Mellon University, 1987.
[31] J.G. Gay and R. Richter, Phys. Rev. Lett. 56 (1986) 2678.